*European Journal of Neuroscience, Vol. 18, pp. 957–968, 2003* 

# Independence of visuotopic representation and orientation map in the visual cortex of the cat

Péter Buzás, Maxim Volgushev, Ulf T. Eysel and Zoltán F. Kisvárday
Institut für Physiologie, Abteilung für Neurophysiologie, Ruhr-Universität Bochum, Universitätsstrasse 150, 44801 Bochum, Germany

*Keywords*: areas 17 and 18, electrophysiology, optical imaging, orientation map, receptive field scatter, visuotopy

## Abstract

The representations of visual space and stimulus orientation were mapped in the cat primary visual cortex using electrophysiological recordings supplemented with intrinsic signal optical imaging. The majority of units displaced up to 600 μm laterally had overlapping RFs both in orientation domains and around singularities of the orientation map. Quantitative comparison of these units revealed only a weak, positive correlation between the difference in their preferred orientations and RF separations (area 17: $r = 0.09$; area 18: $r = 0.15$). The occurrence of nonoverlapping RFs could be accounted for by random RF position scatter rather than by orientation difference between the units. Monte Carlo analysis showed that our findings are compatible with a locally smooth and linear representation of visual space that is not coupled to the representation of stimulus orientation. An important functional implication of the above map relationships is that positional information captured by the retina is faithfully transmitted into the cortex.

## Introduction

Visual sensation begins in the retina where the photoreceptors form a continuous sheet in the back of the eyeball. With the help of the eye optics, the photoreceptor layer captures the image of the outside world – the visual field – without interruptions between the image points except at the location of the optic disc. This positional information is kept in a retinotopic arrangement and transmitted via the thalamus up into the primary visual cortex where it forms a supposedly continuous and smooth representation of the visual field called the visuotopic map (Talbot & Marshall, 1941; Daniel & Whitteridge, 1961; Hubel & Wiesel, 1962, 1974; Bilge *et al*., 1967; Albus, 1975; Tusa *et al*., 1978, 1979; Cowey, 1979; Hetherington & Swindale, 1999; Warren *et al*., 2001; Bosking *et al*., 2002). The only known factor that generates discontinuity of the visuotopic representation is RF position scatter, which varies systematically from central to peripheral representation (Albus, 1975; Cynader *et al*., 1987). As the amount of this scatter (smaller centrally and larger peripherally, Albus, 1975) increases with the RF size of cortical cells and its magnitude difference along the two main visuotopic axes correlates positively with the cortical magnification factor (Cynader *et al*., 1987) the smoothness and continuity of the visuotopic map is, all in all, not affected.

A different scenario is seen for orientation selectivity that emerges, unlike visuotopy, for the first time in the primary visual cortex upon intracortical processing of the thalamic input (reviewed in Vidyasagar *et al*., 1996). The two-dimensional layout of orientation selectivity is periodic to 180° as implied by electrophysiological recordings (Hubel & Wiesel, 1974) and calculated from the Fourier spectra of orientation maps (Cynader *et al*., 1987; Löwel *et al*., 1988). For the most part, the orientation map is continuous and smooth, which can be characterized by a constant rate of change (ROC) of orientation along the lateral dimensions of the cortex. In this regard the orientation map resembles the visuotopic map. However, the smooth zones of the orientation map are interrupted by regions of high ROC of orientation where orientation preference changes rapidly between closely neighbouring cortical locations. These regions can be points often referred to as singularities (Blasdel & Salama, 1986) or pinwheel centres (Bonhoeffer & Grinvald, 1991), or edges of increased ROC, called fractures (Blasdel & Salama, 1986).

In recent years, several attempts have been made to explore the interrelationships between cortical representations of RF attributes using functional imaging (Shmuel & Grinvald, 1996; Crair *et al*., 1997; Hübener *et al*., 1997; Issa *et al*., 2000). These studies provided evidence that local distortion of functional representations is a general feature of cortical map organization. In this respect, the visuotopic map appears to be an exception as it has been considered to lack local discontinuity and be uniformly smooth. This is supported by the notion that visual position is conveyed to the cortex by a strictly retinotopic projection (Hubel & Wiesel, 1963; Sanderson, 1971; Rosenquist *et al*., 1974). Another supporting fact for the smooth and discontinuity-free nature of the visuotopic map is that it is mapped onto the cortex at a much larger scale than any other RF attribute, i.e. it has one period over an entire cortical area. Hence, it does not contribute so much to the 'crowding' of functional maps (Swindale, 1991) that has accounted for the discontinuity in the representation of other RF properties, e.g. orientation selectivity (Swindale *et al*., 2000; Ernst *et al*., 2001). It is thus rather surprising that according to recent reports by Das & Gilbert (1995, 1997, 1999) this notion seems to be broken. By measuring RF position and orientation preferences of nearby cortical cells they found a strong correlation between changes of the two parameters, i.e. RF position shifted proportionally with the difference of orientation preference in cat area 17. Intriguingly, near to singularities where the ROC of orientation preference is the highest, frequently, a complete separation of the RFs of closely neighbouring neurons was seen. While such a relationship between the visuotopic and the orientation maps can be

*Correspondence*: Dr Zoltán F. Kisvárday, as above.
E-mail: kisva@neurop.ruhr-uni-bochum.de

*Received 18 December 2002, revised 21 May 2003, accepted 27 May 2003*

doi:10.1046/j.1460-9568.2003.02808.x

advantageous, for example in processing complex stimulus features (e.g. junctions and corners, Das & Gilbert, 1999) the same map relationship can lead to disadvantageous consequences, for example, the attenuation of visual acuity or even the occurrence of microscotomas.

The present study addresses the question as to whether the above-described relationship between visuotopic and orientation maps represents a common organization principle in areas 17 and 18. Preliminary results have been presented previously in abstract form (Buzás *et al.*, 2001b).

## Materials and methods

For the present investigation, seven adult (8–14 months) cats were used. All surgical procedures were performed in accordance with the German Animal Welfare Act. After initial anaesthesia (ketamin, 7 mg/kg, Ketanest, Parke-Davis, Berlin, Germany and xylazin, 1 mg/kg, Rompun, Bayer Belgium, Sint-Truiden, Belgium; i.m.), the animals underwent surgery for catheter insertion into the femoral artery and for implantion of a tracheal cannula. Prolonged anaesthesia was maintained using artificial ventilation (0.4–0.6% halothane, Halothan Eurim, Eurim-Pharm, Piding, Germany) in a 1 : 2 mixture of $O_2$ and $N_2O$. For muscle relaxation, alcuronium chloride (0.15 mg/kg/h, Alloferin, Hoffman-La Roche, Grenzach-Whylen, Germany) was infused with glucose (24 mg/kg/h, Glucosteril, Fresenius, Bad-Homburg, Germany) and Ringer solution (Ringerlösung Fresenius, Fresenius, Bad-Homburg, Germany). End-tidal $CO_2$ (3–4%), blood pressure (100–140 mmHg) and body temperature (38–39 °C) were monitored continuously. A bilateral craniotomy was made between Horsley–Clarke co-ordinates AP −6 and +9 and LM +0.5 and +6.5. Then, a round stainless steel chamber (31 mm in diameter) was mounted over the exposed cortical region. After removing the dura, the chamber was filled with silicone oil (50 cSt viscosity, Aldrich, Milwaukee, WI, USA) and sealed with a round coverglass.

### *Optical imaging of intrinsic signals*

Optical imaging of intrinsic signals was carried out using the imaging system Imager 2001 (Optical Imaging, Germantown, NY, USA) and the data acquisition software VDAQ-NT (Optical Imaging, Germantown, NY, USA). Prior to optical imaging, correction lenses were applied on the basis of tapetal reflection. The nictitating membranes were retracted and the pupils dilated with 5% phenylephrinhydrochloride (Neosynephrin-POS, Ursapharm, Saarbrücken, Germany) and 1% atropinesulphate (Atropin-POS, Ursapharm, Saarbrücken, Germany), respectively. During data acquisition of intrinsic signals, the camera was focused 650–750 μm below the cortical surface and the cortex was illuminated through the cover glass with a circular fibre optic slit lamp (Schott, Mainz, Germany) surrounding the camera optics (two SMC Pentax lenses, 1 : 1.2, $f = 50$ mm, arranged in a 'tandem' manner, Ratzlaff & Grinvald, 1991) with $609 \pm 5$ nm light (Omega Optical, Brattleboro, VT). Visual stimuli were presented on a video screen (SONY, Pencoed, UK) in 120 Hz noninterlaced mode 28.5 cm in front of the cats' eyes, covering 40–60° of their visual field using the VSG Series Three (Cambridge Research Systems, Rochester, UK) stimulus generator system. The stimulus set consisted of 16 high-contrast, full-field square-wave gratings each drifting in one direction so that the whole set covered 360° in 22.5° steps. The stimuli were displayed in a random sequence at optimal spatial (0.6–1 cycle/deg for area 17 and 0.1–0.2 cycle/deg for area 18) and temporal frequencies (1–2 Hz). Each data acquisition period (during which the stimulus grating moved) was preceded by an interstimulus interval of 10 s when the animals viewed a stationary image of the grating to be presented during the next data acquisition period. Video frames were acquired for 4.5 s, commencing 1 s after the stimulus grating began to move.

### *Analysis of the optical images*

For data analysis, single condition maps (SCMs) were calculated using the Winmix software (Optical Imaging, Germantown, NY, USA). First, images associated with a particular orientation were summed and the result divided by the cocktail blank (i.e. the sum of images associated with any orientations; Bonhoeffer & Grinvald, 1996). The grey value distribution of the resulting images was 'clipped' by discarding extreme values (outside the average ±1.5–3 times the mean absolute deviation). The SCMs were filtered with a Laplace filter (high-pass: 50 pixels, 1064 μm) followed by a boxcar filter (low-pass: 5 pixels, 106 μm). Orientation angle maps were computed using pixel-by-pixel vector-summation of SCMs corresponding to the eight orientations (Blasdel & Salama, 1986; Bonhoeffer & Grinvald, 1991).

### *Extracellular recordings and RF plots*

Multi- or single-unit activity was recorded in the imaged regions using either glass micropipettes (three experiments, inner tip diameter 1–7 μm, filled with 2 M NaCl, 4–10 MΩ) or pairs of epoxy-isolated tungsten microelectrodes (four experiments, 5–12 MΩ, A-M Systems, Sequim, WA, USA). In the latter cases, the electrodes were glued together (250–300 μm lateral tip separation) so that they could be moved simultaneously. All electrode penetrations were made perpendicular to the cortical surface to 1500 μm depth. The minimum response fields of the units were determined using a hand-held visual projector (moving and flashed bars) and plotted onto a tangent screen positioned 57 or 114 cm from the cats' eyes. RFs of only the contra-lateral eye were considered. The retinotopic position, spatial extent (in degrees of visual angle) and preferred orientations were determined for the RF of each unit.

### *Monitoring residual eye movement*

Residual eye movement occurred only seldom and was less than 0.5° of the visual angle. In order to control residual eye movement the following protocols were applied. In five of the seven experiments, after every 2–6 electrode penetrations the fundus of the stimulated eye was projected and plotted onto the tangent screen and the amount of eye movement determined. In the remaining two experiments, a reference electrode was inserted into lamina A1 of the contra-lateral dLGN and a single unit was isolated. Eye movement was determined with high precision by monitoring the RF position of the same thalamic unit before, during and after recording of each cortical unit. Finally, the visual field positions of all units belonging to the same experiment were determined in accordance to residual eye movement using translation and/or rotation for the relative position of the cortical and translation for the relative position of the thalamic units.

### *Statistical analysis*

For a statistical analysis and simulations, we used the SPSS software (SPSS, Chicago, USA). Comparison of the slopes of the regression lines was performed in PRISM (GraphPad Software, San Diego, USA) using the method described by Zar (1999). We also used this method to test the effect of outliers (defined as cases with standardized residuals above 3) on the regression shown in Fig. 2E and F. The slope of the regression lines of the datasets without these outliers did not differ significantly from that of the original sample. Correlation coefficients were calculated by Pearson's correlation.

Orientation scatter of cortical sites was defined as the circular equivalent of standard deviation (Batschelet, 1981). It was computed from the orientation preferences of the $n$ RFs recorded from a

cylindrical cortical volume of 150 μm radius laterally around the site of interest as follows:

$$S = \sqrt{2(1-c)} \quad (1)$$

where $c$ is the length of the mean vector of individual $\alpha_i$ orientation preferences:

$$c = \frac{1}{n}\sqrt{\left(\sum_{i=1}^{n}\cos 2\alpha_i\right)^2 + \left(\sum_{i=1}^{n}\sin 2\alpha_i\right)^2} \quad (2)$$

Thus, orientation scatter ranges between 0 (no scatter) and $\sqrt{2}$ (cancelling orientation angles).

### *Monte Carlo simulations*

We created surrogate normalized RF distance data ($d'$) for comparison with the data of real RF pairs.

Simulation I: The simulated RF locations are indicated by vectors $\mathbf{v}'$, the measured cortical locations by vectors $\mathbf{c}$. Ten normalized RF distance values were created for each real RF pair based on the real cortical locations as follows:

$$d' = \frac{|\mathbf{v}'_1 - \mathbf{v}'_2|}{\overline{a}} = \frac{|(F(\mathbf{c}_1) + \mathbf{r}_1) - (F(\mathbf{c}_2) + \mathbf{r}_2)|}{\overline{a}} \quad (3)$$

where $F$ is the linear visuotopic map, i.e. the best fit linear transformation mapping the measured cortical locations into the measured visual field locations; $\mathbf{r}_1$ and $\mathbf{r}_2$ are random vectors in the visual field accounting for position scatter; $\overline{a}$ is the average diameter of the RF pair. The vectors $\mathbf{r}_1$ and $\mathbf{r}_2$ were drawn randomly from a two-dimensional normal distribution with a mean of zero and equal scatter in elevation and azimuth (SD = 0.43° for area 17, SD = 1.43° for area 18). The total scatter in the simulations was equal to that of the measured RFs (Table 1).

Simulation II: Ten normalized RF distance values were created for each real RF pair based on the real orientation differences ($\delta$) as follows:

$$d' = \frac{|\mathbf{r}_1 - (\mathbf{u} + \mathbf{r}_2)|}{\overline{a}} \quad (4)$$

where the vector $\mathbf{u}$ is given by the co-ordinates $\overline{a} \cdot \delta/90^\circ; 0$. Consequently, if there were no scatter ($\mathbf{r}_1 = \mathbf{r}_2 = 0$), the simulated normalized RF distance would be $d' = \delta/90^\circ$. Note that in simulation II only the RF distances but no explicit visuotopic locations ($\mathbf{v}'$) were simulated.

## Results

Orientation maps were obtained with the intrinsic signal optical imaging technique in areas 17 and 18 (Table 1). Those regions that contained singularities in the orientation angle map were used for a subsequent electrophysiological mapping, while extended linear zones (Shmuel & Grinvald, 2000) where orientation singularities were absent were excluded. This was carried out in order to limit the complexity of our sample as linear zones of the orientation map may underlie different organizing principles than the pinwheel-rich regions (Ohki *et al*., 2000; Shmuel & Grinvald, 2000).

Extracellular recordings were obtained from multi- and single units (area 17: $n = 217$, area 18: $n = 163$, see also Table 1) of closely spaced recording sites (median nearest neighbour distance: 132 μm) whose trajectory was perpendicular to the surface of the cortex. In each electrode penetration (area 17: $n = 97$, area 18: $n = 66$, see also Table 1), 1–4 units were encountered 90–1440 μm below the cortical surface. The extent of the RFs was approximated with rectangles on the basis of the minimum discharge region (Hubel & Wiesel, 1962; Barlow *et al*., 1967) and their orientations were also manually determined using a hand-held projector (see Materials and methods). In the following analysis, RF size of each unit is represented by the diagonal length (diameter) of the RF rectangle and visuotopic location is characterized by the centres of the RFs. On the basis of these parameters, we found that the average size of the RFs in the mapped regions of area 18 (7.9 ± 2.9) was 3.8 times larger than that of area 17 (2.1 ± 0.9, Table 1).

Orientation preference was determined using two independent methods: optical imaging of intrinsic signals and electrophysiology. According to our qualitative observations for the most part of the cortex, there was a generally good correspondence in the measured orientation selectivity between the electrophysiological and the optical imaging results (Fig. 1A). However, in regions of rapidly changing orientation preference, such as around pinwheel centres, an increased mismatch between the two methods was occasionally seen (Fig. 1G). We quantified this relationship by calculating the difference (in the range −90° to +90°) between the preferred orientation of each recorded unit and that of the corresponding pixel position. We found that locations close (up to 150 μm) to pinwheel centres were associated with significantly larger variance of orientation differences ($P < 0.0001$, Levene-test of homogeneity) than sites farther away from pinwheel centres. Therefore we decided to rely on the electrophysiologically determined RF parameters (preferred orientation and RF position) for quantitative purposes and the optical images were used for a qualitative interpretation of the findings.

### *Receptive fields of the recorded units compared to orientation maps*

The arrangement of RFs was studied with regard to the structure of the orientation map as illustrated in Fig. 1. In these exemplary cases, the recorded units are marked by orientated black bars (Fig. 1A and G). To avoid a bias in determining RF orientations, all RF plots were made without prior knowledge of the imaged orientation preference values at their cortical locations. The majority of the penetrations were located in orientation domains where the surrounding regions had similar orientation preferences, i.e. the same colour in the angle map (see for example penetrations numbers 13, 15, 30 in Fig. 1A; 2, 11, 26 in Fig. 1G). Other penetrations were located near to singularities where the representation of all orientations met in a pinwheel manner and thus the orientation preferences of closely neighbouring locations could differ up to 90°. When we superimposed the RF contours of all units in the co-ordinate system of the visual field, it could be readily seen that most but not all of them overlapped with each other. Our first general observation was that units separated by less than 750 μm tended to have overlapping RFs. This was true not only in situations when the neighbouring locations had similar (Fig. 1C) or different orientations (Fig. 1D, E and F) even when the orientation preference changed rapidly over a short lateral distance (Fig. 1J and L). Occasionally, little or no overlap was found between the RFs of close-by units, independently of their orientation preferences (e.g. Fig. 1C, D, J and K). Such cases occurred in all layers and constituted only the minority of our sample.

### *Relationship between receptive field shift and cortical distance*

For a quantitative analysis of the relationship between RF position and cortical distance, the recorded units were compared to each other pairwise. To this, a careful alignment of the location of each unit's RF in the visual field was necessary together with a precise knowledge about the cortical position of the recording electrodes (see Materials and methods). Only those pairs whose lateral cortical separation did not

TABLE 1A. Summary of the electrophysiological data

| | Area 17 (4 animals, 217 RFs) | | | Area 18 (3 animals, 163 RFs) | | |
|---|---|---|---|---|---|---|
| | Minimum | Maximum | Mean ± SD | Minimum | Maximum | Mean ± SD |
| Cortical depth of recordings (μm) | 92 | 1397 | 703 ± 273 | 90 | 1440 | 720 ± 304 |
| RF centre azimuth (deg) | −3.7 | +2.3 | −0.8 ± 1.6 | −3.6 | +10.1 | +2.4 ± 2.5 |
| RF centre elevation (deg) | −1.8 | +3.1 | +0.78 ± 1.06 | −23.3 | −10.3 | −15.06 ± 3.17 |
| RF diameter (deg) | 0.4 | 5.1 | 2.1 ± 0.9 | 1.0 | 14.6 | 7.9 ± 2.9 |

TABLE 1B. RF position scatter

| | Area 17 (4 animals, 217 RFs) | Area 18 (3 animals, 163 RFs) |
|---|---|---|
| Horizontal scatter (deg) | 0.43 | 1.70 |
| Vertical scatter (deg) | 0.42 | 1.09 |
| Total scatter (deg) | 0.60 | 2.02 |

TABLE 2. Statistical analysis of RF pairs

| | | | Simulated data | | | |
|---|---|---|---|---|---|---|
| | Real data | | Simulation I: linear VT map + scatter | | Simulation II: 1RF/90° + scatter | |
| RF position data | Area 17 | Area 18 | Area 17 | Area 18 | Area 17 | Area 18 |
| No. of RF pairs | 2527 | 2487 | 25270 | 24870 | 25270 | 24870 |
| Normalized RF distance vs. cortical distance: RF diameters/mm (Fig. 2E and F) | | | | | | |
| slope ± SEM | 0.315 ± 0.031 | 0.384 ± 0.027 | $0.144 \pm 1.1 \times 10^{-5}$ | $0.262 \pm 9.3 \times 10^{-6}$ | $0.203 \pm 1.3 \times 10^{-5}$ | $0.330 \pm 1.2 \times 10^{-5}$ |
| r | 0.20 | 0.27 | 0.08 | 0.18 | 0.10 | 0.17 |
| Normalized RF distance vs. orientation difference: RF diameters/degrees (Fig. 4A and B) | | | | | | |
| slope ± SEM | $0.00093 \pm 2.1 \times 10^{-4}$ ($0.0106 \pm 5.7 \times 10^{-4}$*) | $0.0013 \pm 1.8 \times 10^{-4}$ | $0.00033 \pm 7.0 \times 10^{-5}$ | $0.00035 \pm 6.2 \times 10^{-5}$ | $0.0079 \pm 7.1 \times 10^{-5}$ | $0.0080 \pm 6.3 \times 10^{-5}$ |
| r | 0.09 (0.84*) | 0.15 | 0.03 | 0.04 | 0.58 | 0.63 |
| Normalized ROC of RF position vs. ROC of orientation: RF diameters/degrees (Fig. 4C and D) | | | | | | |
| slope ± SEM | $0.0042 \pm 0.00016$ ($0.0110 \pm 6.6 \times 10^{-4}$*) | $0.0028 \pm 1.5 \times 10^{-4}$ | $0.0042 \pm 5.8 \times 10^{-5}$ | $0.0031 \pm 5.4 \times 10^{-5}$ | $0.0111 \pm 5.7 \times 10^{-5}$ | $0.0107 \pm 5.6 \times 10^{-5}$ |
| r | 0.48 (0.81*) | 0.37 | 0.42 | 0.35 | 0.78 | 0.78 |

All correlations and regression coefficients are significant ($P < 0.01$). *Data taken from Das & Gilbert (1997).

 

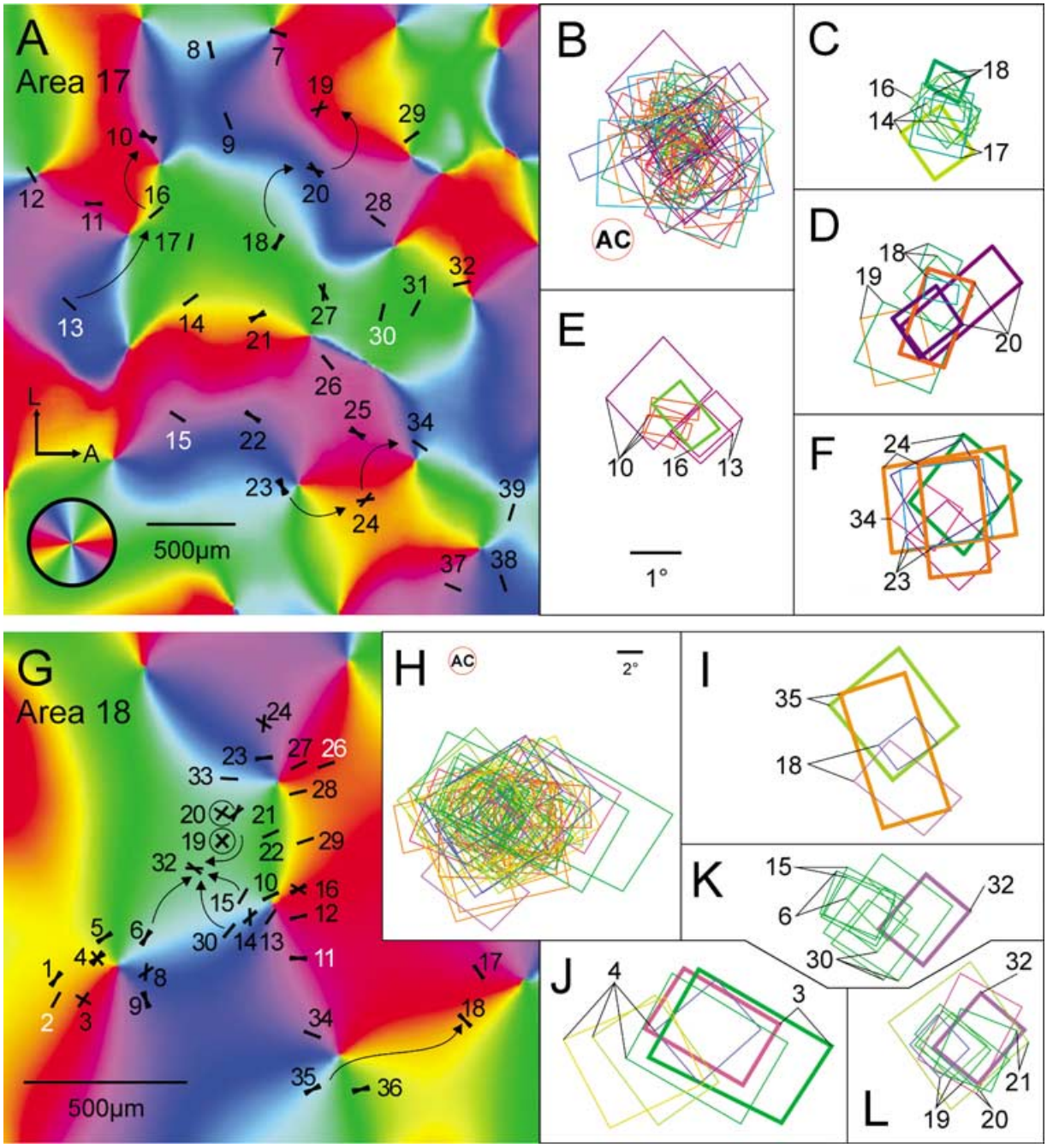


FIG. 1. Comparison between RF position and orientation in area 17 (A–F) and area 18 (G–L). (A and G) Comparison between orientation preferences determined by electrophysiological recordings (altogether 30 penetration sites in A and 32 in G, numbering refers to the experimental notes) and orientation maps obtained with the intrinsic signal optical imaging technique (see inset for colour-code of orientation). Each bar represents a recorded unit ($n = 67$ in A, $n = 77$ in G). In most cases, several units were recorded along the same penetration. Note that the orientation preferences determined by optical imaging do not always fit with individual unit responses. White numbers indicate examples of penetrations in orientation domains. Panels B–F and H–L show the superimposition of RFs (rectangles) of units in A and G, respectively. The orientation selectivity of each RF contour derived from spike responses is indicated by colour corresponding to the colour coding of the orientation map. Numbers refer to penetrations in A and G. (B and H) All RFs are superimposed with respect to the visuotopic location of area centralis (AC). (C) RFs of neighbouring units recorded in the same orientation domain. There are overlapping (thin contours) and nonoverlapping (thick contours) RFs. (D–F) Examples of penetration sequences (arrowed in A) where the orientation preference changed in a $0°-90°-0°$ fashion. For each sequence, RFs belonging to intermediate penetrations are drawn in thick lines. Note that the RFs of the intermediate penetrations (D, 20; E, 16; F, 24) overlap substantially with each of the orthogonally orientated and flanking neighbours whereas there is little or no overlap between the RFs of the flanks which are iso-orientated to each other. Importantly, such a relationship could be generally found in any part of the orientation map comprising orientation domain (D) and centre regions (E and F). (I) Orthogonally orientated and overlapping RFs which were found on opposite sides of a pinwheel centre (arrowed in G). (J) Orthogonally orientated RFs showing various extent of overlap. (K) Some units (thin RF contours) neighbouring on site 32 (thick RF contour) had orthogonal orientation preferences and most of them showed little overlap. (L) Other units (thin RF contours) neighbouring on site 32 (thick RF contour) had orthogonal orientation preferences but overlapping RFs. Sites 19 and 20 (encircled in G) each contained units having orthogonal and overlapping RFs. A, anterior; L, lateral.

exceed 600 μm were taken into account. This distance corresponds approximately to half of the average spatial wavelength of the orientation map (Swindale *et al.*, 1987; Löwel *et al.*, 1988; Buzás *et al.*, 2001a). By using this distance limit, we aimed to ensure an unambiguous measure of distance in the orientation map. Figure 2A and B illustrates the relationship of the absolute RF distance to lateral cortical separation in the two mapped areas. These graphs suggest that RF distance increases monotonically with cortical separation. For the sake of simplicity, the relationship was approximated as being closely linear (Pearson's correlation: $r = 0.23$ for area 17 and $r = 0.26$ for area 18). We were also interested to know the average rate of change (ROC) of RF position per unit cortical distance provided by the slopes of the regression lines. The resulting value of 0.67 deg/mm for area 17 is consistent with the high magnification factor described here (Albus, 1975; Tusa *et al.*, 1978). For area 18, the movement of RF centres was found to be 2.58 deg/mm which corresponds to the magnification factor described for approximately $-15^\circ$ elevation (Tusa *et al.*, 1979). Thus, the average ROCs of RF centre positions in the two areas reveals a 3.85-fold difference. Note that this figure is very close to the ratio of RF sizes (3.8) of the two areas (Figs 2C and D). The wider range of eccentricities and wider distribution of RF sizes (Table 1) in the area 18 sample suggests that the cortical magnification factor had a larger variation here than in the area 17 sample. This explains the presence of outliers in Fig. 2B.

In order to make the two data sets directly comparable to each other, we normalized the centre-to-centre distances by dividing them by the average diameter of each RF pair. The resulting values showed, again, a closely linear relationship to the lateral distance of the penetrations (Fig. 2E and F; Pearson's correlation: $r = 0.20$ for area 17 and $r = 0.27$ for area 18). Importantly, the slopes of the regression lines belonging to the two areas did not differ statistically from each other ($P > 0.09$). From these plots, one can readily approximate the amount of move on the cortical surface that is required to find nonoverlapping RFs. This distance, where the regression line reaches 1, is 2.107 mm in area 17 and 2.007 mm in area 18 (Fig. 2E and F). It should be noted that the outliers in the normalized data set did not have any significant effect on the slopes of the regression lines (see Materials and methods). On the other hand, it is also clear, that RF distances of unit pairs show considerable scatter around the mean indicating that certain pairs had nonoverlapping RFs even when their cortical separation was as small as 100 μm.

### *Position scatter and its relationship to orientation scatter*

As Hubel & Wiesel (1974) originally described, there is a difference between the RF locations of closely neighbouring neurons that is called RF position scatter. Here we assumed a linear visuotopic map that was derived by applying linear regression (separately for each animal) on the measured cortical position vs. visual field position pairs. We displayed RF deviations in azimuth and elevation from their predicted positions for all recorded units, separately for area 17 (Fig. 3A) and area 18 (Fig. 3B). The horizontal and vertical deviations showed normal distributions (Kolmogorov–Smirnov test, $P > 0.05$). In order to quantify the RF position scatter, we calculated the SD of RF deviations along the visual field axes (Table 1). Interestingly, while in area 17 there was no statistical difference between the horizontal and vertical scatter components ($SD_{hor} = 0.43^\circ$, $SD_{ver} = 0.42^\circ$, Levene-test of homogeneity, $P > 0.8$) area 18 showed significantly larger scatter in the horizontal than in the vertical dimension ($SD_{hor} = 1.70^\circ$, $SD_{ver} = 1.09^\circ$, $P < 0.01$).

The above calculations showed that the RF scatter was globally random, i.e. when all recorded units of large cortical regions were pooled. We wanted to know whether this scatter correlates with the scatter of orientation measured at corresponding positions. We hypothesized that the covariation of the two types of scatter with each other would be a signature of the interdependence of the visuotopic and orientation maps. Therefore, in the subsequent analysis, the deviation of RF locations was compared to the local orientation scatter (Fig. 3C and D). The deviation of each RF from its predicted location was characterized by their distance (Euclidean) in the visual field. Orientation scatter was defined for each recorded unit as the standard deviation (see Materials and methods) of the orientation preferences of all units within 150 μm lateral distance. The scatter plots comparing the above two measures of 'disorder' are displayed in Fig. 3C and D. It is readily seen that the data points are almost uniformly distributed. Importantly, there was no significant correlation between RF deviation and orientation scatter.

### *RF movement compared to orientation shift*

The above findings on the RF position scatter vs. orientation scatter indicated so far no direct relationship between visuotopic and orientation maps. In order to address this issue more generally and from the point of view of the structure of the orientation map, the normalized RF shifts between the unit-pairs were plotted against the difference of their orientation preferences (Fig. 4A and B). The resulting graphs showed no obvious change of RF distance associated with the orientation difference. The flat slope of the regression lines (solid lines, see Table 2 for regression coefficients) suggested only a small (0.08 RF diameters for area 17, 0.12 RF diameters for area 18) increase of RF distance between iso- and cross-orientated RF pairs. This led us to the supposition that orientation and position are mapped rather independently on the cortex.

On asserting this finding we created surrogate values of normalized RF distance using Monte Carlo simulation (for details see Materials and methods). Orientation preference values were taken from the measured data without imposing any particular structure of the orientation map. The simulations were based on two different hypotheses about the relationship of visuotopic and orientation maps. In simulation I, we proposed a linear visuotopic map that was (i) constructed by a linear approximation of our measurement points and (ii) uncorrelated to the orientation map. To account for position scatter, we added the same amount of random scatter as found in our real data set. The regression line of the resulting RF distance vs. orientation difference pairs was then calculated (broken lines in Fig. 4A and B). It is clearly seen that the slopes of the regression lines obtained from the simulated data and those of the real data are very similar (see also Table 2). Simulation II was based on the proposition that orthogonally orientated RFs tend to be nonoverlapping that is equivalent with the following formula: normalized RF distance = orientation difference/90 deg. This model has emerged recently on the basis of experimental data (Das & Gilbert, 1997) and theoretical considerations (Ernst *et al.*, 2001). In testing our data against such a model, it is important to examine whether the RF position scatter can obscure any strong correlation between RF shift and orientation difference. Therefore, we simulated the RF distance for each unit pair from the measured orientation difference using the above equation and added random position scatter as in simulation I. The regression line of the simulated RF distance vs. orientation difference pairs is shown for comparison in Fig. 4A and B (stippled lines). Contrary to the real data and simulation I, in which RF position and orientation preference were conjectured as independent attributes, the slopes deriving from the latter simulation were much steeper (Table 2). Thus, our findings are consistent with independent visuotopic and orientation maps. In addition to this, the above findings were compared to available data of the map relationships in area 17 published by Das & Gilbert (1997). In Fig. 4A, the thin line shows the

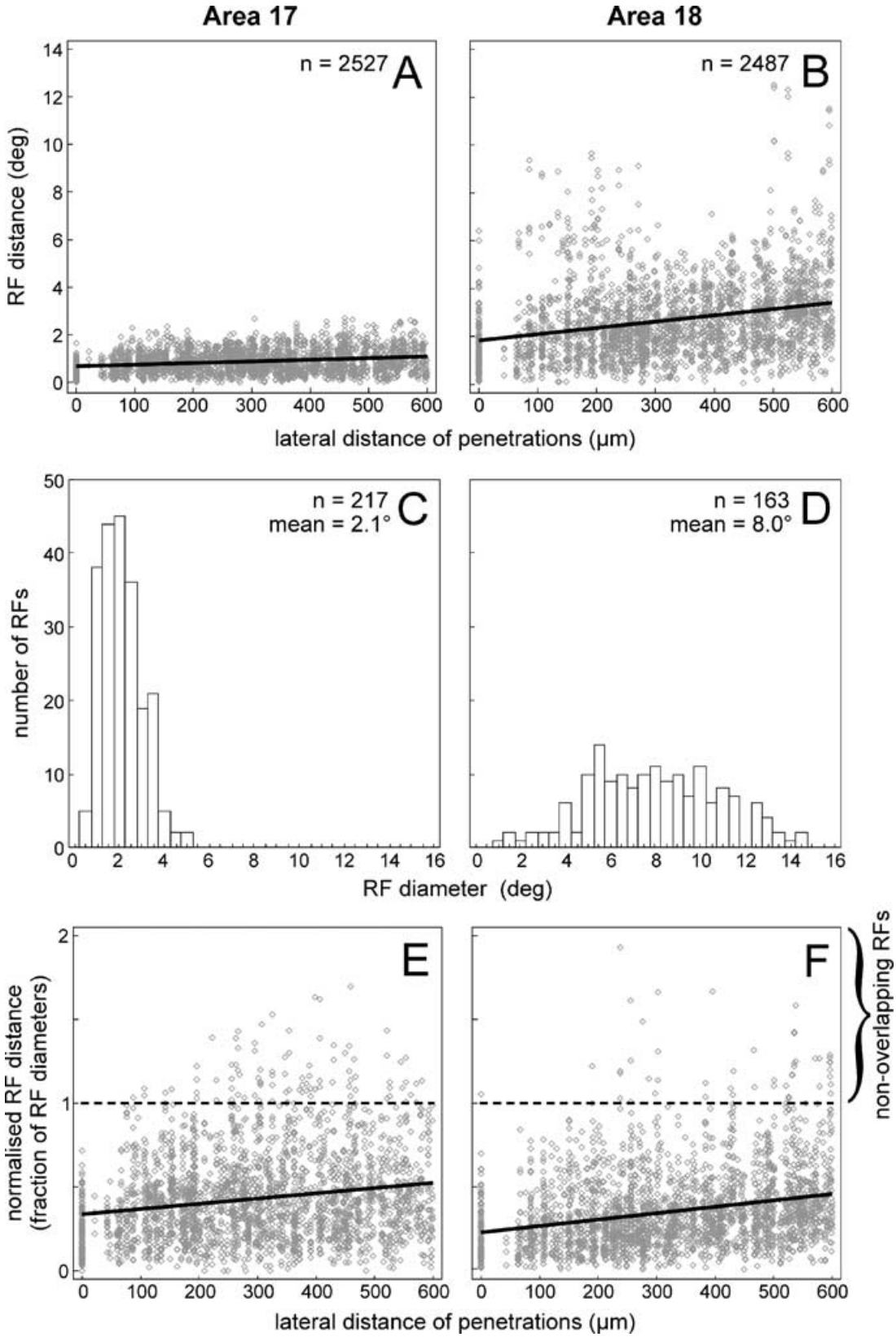


FIG. 2. Cortical separation and RF distance for pairs of recorded units show a weak positive correlation. The slopes of the regression lines suggest that RF centres shift by 0.67 deg/mm in area 17 (A) and 2.58 deg/mm in area 18 (B) on average. The distribution of RF sizes (represented by diagonal length) were Gaussian shaped in the two areas (C and D). Normalization of the RF distance by the average RF size for each unit-pair allowed a direct comparison between the area 17 and area 18 data (E and F). As calculated from the slopes, a lateral movement of approximately 2 mm in the cortex results in nonoverlapping RF locations in both areas.

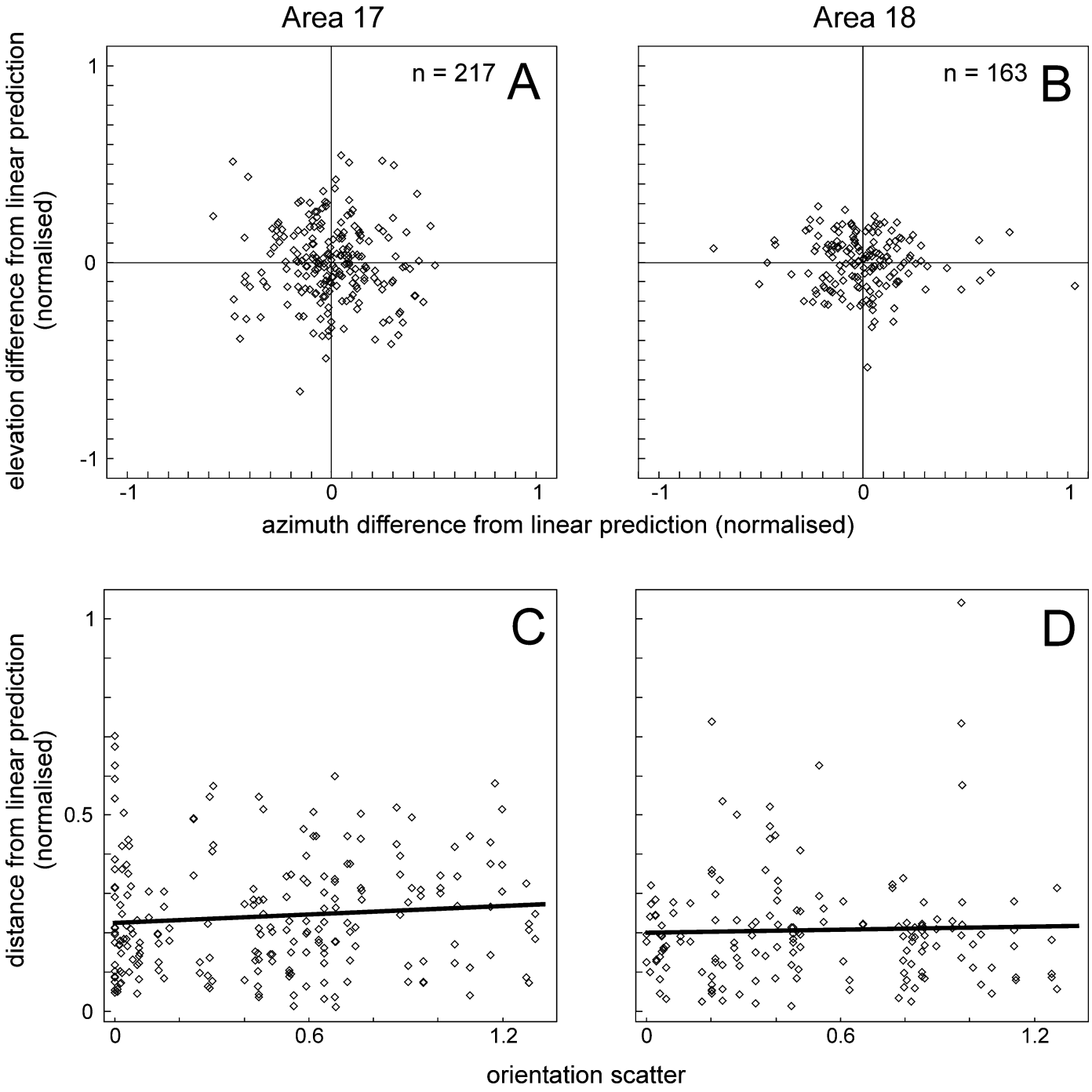


FIG. 3. Residual analysis does not show distortions of the retinotopic map in regions of increased orientation scatter. (A and B). Scatter plots showing the distribution of the measured RF centres (normalized to mean RF diameter of the corresponding area, see Table 1) relative to their predicted positions (0.0; 0.0) based on a linear approximation of the retinotopic map. The scatter plot reveals normally distributed random scatter along both visual field axes. The horizontal scatter in area 18 (B) is slightly higher than the vertical scatter. (C and D) Graphs comparing the deviation in RF position (*y*-axis) to orientation scatter (*x*-axis). The absolute (Euclidean) distance from the position predicted by linear approximation of the retinotopic map is largely independent from the local orientation scatter (area 17: $r = 0.093$; area 18: $r = 0.035$ nonsignificant correlations).

regression line deriving from their measurements. Clearly, the slope of this regression line ($0.0106 \pm 0.00057$) is approximately ten times higher than that of our measured data ($0.00093 \pm 0.00021$ for area 17) whereas it matches well with that of simulation II assuming strongly coupled maps in which locations of orthogonal orientation preferences possess nonoverlapping RFs ($0.0079 \pm 0.000071$ for area 17). This also implies that the random position scatter observed in our measurements was insufficient to obscure a strong interdependence of the two types of map such as that inferred from the data of Das & Gilbert (1997).

The dependence of RF shift from the orientation shift was also compared for different cortical depths. For this purpose, the data were divided into two groups. The first group represented unit pairs, which were not deeper than 500 μm from the cortical surface. The second

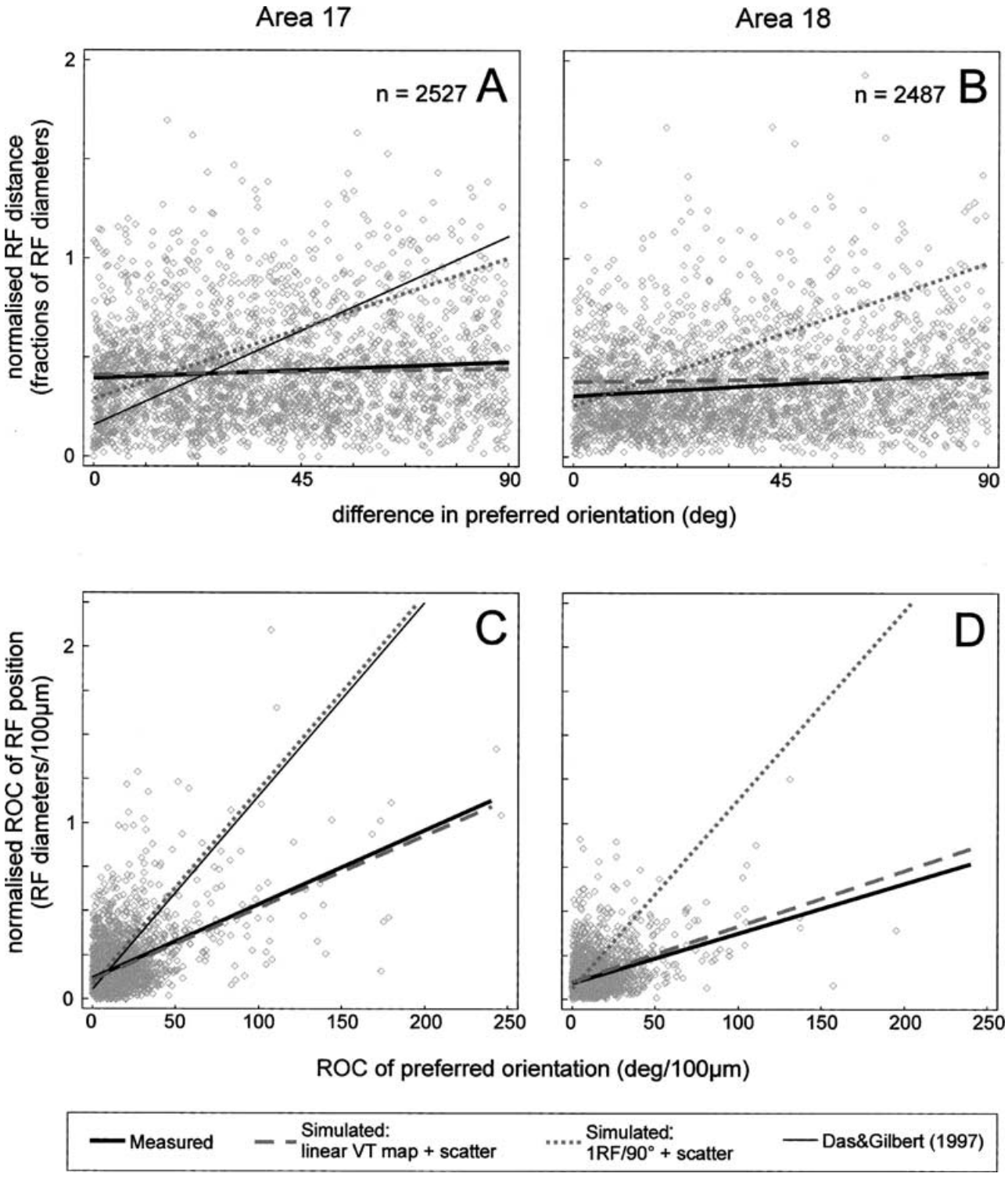


FIG. 4. Scatter plots and linear regression showing the independence of orientation and RF position shift of experimentally measured RF pairs and comparison to Monte Carlo simulations. (A and B) Receptive field separation does not depend on the difference of orientation preferences. The regression of the measured data (thick lines) was similar to that of simulation I, assuming linear visuotopic map plus realistic position scatter (broken lines). Simulation II, supposing nonoverlapping RFs for orthogonal orientations and realistic position scatter, yielded radically different results (stippled lines). For comparison, thin line indicates data of area 17 reported by Das & Gilbert (1997) that is at variance with our finding but agrees well with simulation II. (C and D) The positive regression of the measured ROC of orientation preferences and RF positions (thick lines) is an artefact produced by the calculation of ROC rather than originating from the relationship of the maps (see text for detail). Such a spurious positive regression is also present in simulation I (broken lines) where the visuotopic map is considered to be independent of the orientation map. A much steeper positive regression is seen for the alternative model (simulation II) which assumes nonoverlapping RFs between cortical locations of orthogonal orientations and the same amount of RF position scatter as above (stippled lines). For comparison, thin line indicates data of area 17 reported by Das & Gilbert (1997).

group included unit pairs, which were located 500–1500 μm from the cortical surface. A statistical comparison of the slopes of the regression lines calculated for these groups revealed no significant difference ($P > 0.84$ for area 17, $P > 0.75$ for area 18) indicating that the observed tendencies are the same for the entire data of all laminae.

A central part of the observations of Das & Gilbert (1997) was a strong positive correlation between the ROC of RF movement and the ROC of preferred orientation for pairs of RFs. We also applied the same analysis to our measured data but expected a weak correlation on the basis of Fig. 3C and D. However, we observed a monotonical increase in the rate of RF movement with the rate of orientation shift for the RF pairs (positive correlation, Table 2, thick lines in Fig. 4C and D). What is the source of this correlation? It is the result of the calculations of the ROC values and should not be interpreted as a correlation between the spatial gradients of the two maps. Indeed, both the ROC of RF position and the ROC of orientation preferences were obtained, respectively, by dividing RF position differences and orientation differences by the cortical distance of the units. Importantly, the resulting values along both axes of Fig. 4C and D must be inversely proportional to the same cortical distance that, in turn produces a strong positive correlation. This effect is clearly seen in the results of Monte Carlo simulation I (broken lines in Fig. 4C and D). Here, the visuotopic locations were defined as independent of the orientation map, nonetheless the calculated ROC values were positively correlated (Table 2). In other words, simulation I provided a 'baseline level' of linear dependence of the ROC values that should be considered as spurious and be taken into account when data sets are compared to each other. As seen in Fig. 4C and D, the regression lines of our experimental data show virtually identical slopes with the 'baseline' implying no dependence between visuotopy and orientation preference. For comparison, we evaluated the data set of simulation II in which a complete separation of orthogonally orientated RFs (plus realistic scatter) was conjectured. The accompanying regression lines (stippled lines in Fig. 4C and D) clearly show that this model cannot explain our measured data although it is compatible with those of Das & Gilbert (1997; thin line in Fig. 4C).

## Discussion

The main finding of this study is that the visuotopic map of areas 17 and 18 of the cat is locally smooth including locations where the orientation map shows an increased rate of change or even discontinuities. In this regard, our findings corroborate earlier experimental data on the smooth and continuous representation of visual field positions (Hubel & Wiesel, 1974; Albus, 1975; Tusa *et al*., 1978; Hetherington & Swindale, 1999). However, they disagree with recent studies, which found a systematic relationship in the arrangement of distortions between visuotopic and orientation preference maps (Durbin & Mitchison, 1990; Das & Gilbert, 1995, 1997, 1999).

### *Technical considerations*

Before interpreting our results, a few technical issues need to be taken into account. A potential error in measuring the relative position of RFs is related to residual eye movements (see Materials and methods). We noticed that under low-level anaesthesia (<0.4% halothane) residual eye movement occurs more frequently and with higher amplitude than under deep anaesthesia (>0.4% halothane; P. Buzás, U. T. Eysel & Z. F. Kisvárday, unpublished observation). In the present study, using 0.4–0.6% halothane, residual eye movement occurred approximately once per 10 min and had, typically, 0.2° amplitude. Obviously, this can cause only a negligible error in assessing RF positions as a 0.2° shift represents approximately 1/10 and 1/40, respectively, of the average RF diameter of our area 17 and area 18 units.

Recording multiunit activity is another potential source of measurement error. The possible effects include increased position scatter (see below) and increased RF area. Each of them would result in an overestimation of RF overlap between neighbouring units including those with orthogonal orientation preference. However, they would not affect the average RF distances at any orientation difference. Thus a correlation between RF shift and orientation difference could not be masked.

Finally, the normalized RF centre-to-centre distance as a measure of RF separation needs to be discussed. We emphasize that this measure is, in fact, an indirect indication of RF overlap. This is so because RF overlap depends on the aspect ratio and relative size and orientation of the two RFs, in addition to the normalized RF distance. By the same token, the same RF distance can mean different proportions of overlap, depending on the above factors. On the basis of geometrical relationships between pairs of RFs (approximated by ellipses) it can be conceived that the normalized RF distances above 1 represent non-overlapping RFs. Because most of the RFs in our sample had an aspect ratio of close to 1 (see Fig. 1), the normalized RF distance of 1 represents a threshold of spatial overlap (see Fig. 2E and F). Note that the conservative threshold of overlap can be below 1 for a small number of elongated RF pairs. In the most important case of orthogonally orientated RFs, however, the threshold is not lower than 0.5 RF diameter, even if an aspect ratio of 0 (infinitely thin RFs) is assumed (strictly valid only for RFs of equal size).

### *Comparison to previous findings on the organization of the visuotopic map*

Our data clearly deviate from the results reported by Das & Gilbert (1997). They found a strong correlation between the change in visuotopic location and preferred orientation that was most evident near to pinwheel centres. We did not find such a relationship between visuotopic and orientation maps. Instead, our findings indicate a smooth cortical representation of the visual field (Hubel & Wiesel, 1974; Albus, 1975; Tusa *et al*., 1978, 1979; Warren *et al*., 2001) with no correlation to the orientation map. Although we used similar approaches to Das and Gilbert's study there are some important differences. First, our recorded units were sampled from all cortical layers whereas theirs were derived from the superficial layers. We think that this alone cannot account for the differences because our data filtered for the superficial layers showed similar results to that of the deep layers. Second, it should be emphasized that RF size measurement alone can put a significant effect on the results because smaller RFs give rise to stronger RF separation than large RFs across the same cortical distance. Our area 17 RFs had a mean width of 1.5° (assuming square shape and 2.1° average diameter) while their RFs, with a few exceptions, were smaller than 1°. This suggests that the two studies either sampled visuotopically different regions of area 17 and/or that subjective factors in determining RF boundaries played a role. Third, the data presented here for areas 17 and 18 showed a much larger RF position scatter than that inferred from the data of Das & Gilbert (1997). Some of this scatter originates from technical sources such as remaining misalignment of RFs that cannot be avoided. Such random scatter could have the consequence that we underestimate the correlation between RF shift and orientation difference (see Fig. 4A and B). We addressed this possibility in the second Monte Carlo simulation where we forced orthogonal RFs being nonoverlapped and examined the effect of the scatter known to be present in the data. The results showed that this position scatter would be insufficient to obscure such a strong interdependence of visuotopic and orientation maps (see Fig. 4A and B).

Recently, Hetherington & Swindale (1999) arrived at a similar conclusion to ours using tetrode-recordings for determining spatial

position scatter and orientation scatter of neighbouring single units. Although they could not compare their data to orientation maps, they found that units even with very dissimilar preferred orientations had only slightly larger RF position separation than those of other unit pairs. Further support for the independence of the visuotopic map from the orientation map comes from optical imaging studies of the ferret visual cortex (Bosking *et al*., 2002). This study showed that visual space is orderly represented at a fine scale without local relationships with the orientation map. Our data presented here provide strong support for such a conclusion in the primary visual cortex of the cat.

### *Considerations on the relationship between the visuotopic representation and functional maps*

A characteristic feature of the visual cortex is that it accommodates a multitude of maps of various response properties each representing a particular parameter of the visual world (position, orientation, colour, etc.). A cardinal issue – also known as the dimension reduction problem – is how this multidimensional parameter space is transformed on to the essentially two-dimensional cortical sheet. In general, coverage uniformity and continuity are two oppositely acting constrains which have been assumed to underlie map formations (Hubel & Wiesel, 1977; Swindale, 1991; see also Swindale *et al*., 2000). There are two conflicting views with regard to the mechanisms by which local distortions – decreased continuity- help to maintain maximal coverage. According to one theory, the distortions caused by one (or some) of the stimulus parameters (e.g. orientation) would be accompanied by a higher resolution of the other stimulus parameters in the same cortical location. For example, translated for the known structure of the orientation map: in singularities, a 'rough' representation whereas in orientation domains a 'fine' representation of orientation preferences is seen. An implementation of the above cost function is a visuotopic map that has a fine resolution in singularities and, in turn, a coarse resolution in orientation domains (Durbin & Mitchison, 1990). This organization scheme is attractive as it can minimize the neuronal wiring required for local operations. However, it can be disadvantageous because by increasing the number of parameter maps, more and more cortical area must be devoted to map distortions. A possible solution to this problem is offered by the alternative theory according to which the distortions belonging to different maps would be arranged in a correlated manner. These locations, where a continuous representation cannot be fulfilled, will be concentrated in limited regions around which the representation can remain highly continuous. It is conceivable that such a scenario will generate 'by-products' in the form of spatially distributed 'holes' where certain RF characteristics are underrepresented (nonoptimal coverage) or even absent. These locations can be considered as the 'victims' of a trade-off between different maps in organizing and keeping local distortions to a minimum.

The data reported by Das & Gilbert (1997) showing correlated distortions of RF position and preferred orientation maps support such a view. Pursuing this idea further, they suggest that the close proximity of neurons with radically different RF parameters can be utilized for higher processing, e.g. the representation of corners and T-shapes (Das & Gilbert, 1999). While our findings generally do not refuse the possible existence of the above mechanisms they disagree with the presence of discontinuities in the visuotopic map. Whether complex stimulus features possess a spatially ordered representation in the primary visual cortex remains an exciting matter of further investigations.

It should be noted that RF position scatter could have an important bearing in preserving the completeness of the visuotopic representation. Suppose that nature's solution to the dimension reduction problem necessitates the under-representation of certain locations in the visual field. Obviously, random position scatter can smooth the visuotopic map in a manner such that the under-represented locations will be covered by RFs.

Finally, we assume that the smooth and continuous character of the visuotopic map as observed here is related to its fundamental role. The map of visual space in primary visual cortical areas constitutes a framework of the outside world on which 'low-level' RF modalities (e.g. orientation and direction selectivity) are built and then, can be combined in 'higher-level' mechanisms such as implied by the gestalt principles. Hence, a complete coverage of visual space is likely to be a prerequisite of perceptual completeness.

## Acknowledgements

Authors thank Ms Éva Tóth and Mrs Christa-Tacke for their excellent technical assistance. We also thank Mr Alex Ferecskó and Ms. Krisztina Kovács for their help during the experiments. This work was supported by the Deutsche Forschungsgemeinschaft (SFB 509 TP/A6 to Z.F.K and SFB 509 TP/A5 to M.V).

## References

Albus, K. (1975) A quantitative study of the projection area of the central and paracentral visual field in area 17 of the cat. *Exp. Brain Res.*, **24**, 159–179.
Barlow, H.B., Blakemore, C. & Pettigrew, J.D. (1967) The neural mechanism of binocular depth discrimination. *J. Physiol. (Lond.)*, **193**, 327–342.
Batschelet, E. (1981) *Circular Statistics in Biology.* Academic Press, London.
Bilge, M., Bingle, A., Seneviratne, K.N. & Whitteridge, D. (1967) A map of the visual cortex in the cat. *J. Physiol. (Lond.)*, **191**, 116–118.
Blasdel, G.G. & Salama, G. (1986) Voltage-sensitive dyes reveal a modular organization in monkey striate cortex. *Nature*, **321**, 579–585.
Bonhoeffer, T. & Grinvald, A. (1991) Iso-orientation domains in cat visual cortex are arranged in pinwheel-like patterns. *Nature*, **353**, 429–431.
Bonhoeffer, T. & Grinvald, A. (1996) Optical imaging based on intrinsic signals. The methodology. In Toga, A.W. & Mazziotta, J.C., (Eds), *Brain Mapping: the Methods*, Academic Press, San Diego, pp. 55–97.
Bosking, W.H., Crowley, J.C. & Fitzpatrick, D. (2002) Spatial coding of position and orientation in primary visual cortex. *Nature Neurosci.*, **5**, 874–882.
Buzás, P., Eysel, U.T., Adorján, P. & Kisvárday, Z.F. (2001a) Axonal topography of cortical basket cells in relation to orientation, direction, and ocular dominance maps. *J. Comp. Neurol.*, **437**, 259–285.
Buzás, P., Volgushev, M., Eysel, U.T. & Kisvárday, Z.F. (2001b) Relationship between receptive field scatter and orientation map in the cat visual cortex. *Soc. Neurosci. Abstr.*, **27**, 748.
Cowey, A. (1979) Cortical maps and visual perception. The Grindley Memorial Lecture. *Quart. J. Exp. Psychol.*, **31**, 1–17.
Crair, M.C., Ruthazer, E.S., Gillespie, D.C. & Stryker, M.P. (1997) Ocular dominance peaks at pinwheel center singularities of the orientation map in cat visual cortex. *J. Neurophysiol.*, **77**, 3381–3385.
Cynader, M.S., Swindale, N.W. & Matsubara, J.A. (1987) Functional topography in cat area 18. *J. Neurosci.*, **7**, 1401–1413.
Daniel, M. & Whitteridge, D. (1961) The representation of the visual field on the cerebral cortex in monkeys. *J. Physiol.*, **159**, 203–221.
Das, A. & Gilbert, C.D. (1995) Long-range horizontal connections and their role in cortical reorganization revealed by optical recording of cat primary visual cortex. *Nature*, **375**, 780–784.
Das, A. & Gilbert, C.D. (1997) Distortions of visuotopic map match orientation singularities in primary visual cortex. *Nature*, **387**, 594–598.
Das, A. & Gilbert, C.D. (1999) Topography of contextual modulations mediated by short-range interactions in primary visual cortex. *Nature*, **399**, 655–661.
Durbin, R. & Mitchison, G. (1990) A dimension reduction framework for understanding cortical maps. *Nature*, **343**, 644–647.
Ernst, U.A., Pawelzik, K.R., Sahar-Pikielny, C. & Tsodyks, M.V. (2001) Intracortical origin of visual maps. *Nature Neurosci.*, **4**, 431–436.
Hetherington, P.A. & Swindale, N.V. (1999) Receptive field and orientation scatter studied by tetrode recordings in cat area 17. *Visual Neurosci.*, **16**, 637–652.
Hubel, D.H. & Wiesel, T.N. (1962) Receptive fields, binocular interaction and functional architecture in the cat's visual cortex. *J. Physiol. (Lond.)*, **160**, 106–154.

Hubel, D.H. & Wiesel, T.N. (1963) Receptive fields of cells in striate cortex of very young, visually inexperienced kittens. *J. Neurophysiol.*, **26**, 994–1002.

Hubel, D.H. & Wiesel, T.N. (1974) Uniformity of monkey striate cortex: a parallel relationship between field size, scatter, and magnification factor. *J. Comp. Neurol.*, **158**, 295–305.

Hubel, D.H. & Wiesel, T.N. (1977) Ferrier lecture. Functional architecture of macaque monkey visual cortex. *Proc. R. Soc. Lond. B.*, **198**, 1–59.

Hübener, M., Shoham, D., Grinvald, A. & Bonhoeffer, T. (1997) Spatial relationships among three columnar systems in cat area 17. *J. Neurosci.*, **17**, 9270–9284.

Issa, N.P., Trepel, C. & Stryker, M.P. (2000) Spatial frequency maps in cat visual cortex. *J. Neurosci.*, **20**, 8504–8514.

Löwel, S., Bischof, H.J., Leutenecker, B. & Singer, W. (1988) Topographic relations between ocular dominance and orientation columns in the cat striate cortex. *Exp. Brain Res.*, **71**, 33–46.

Ohki, K., Matsuda, Y., Ajima, A., Kim, D.S. & Tanaka, S. (2000) Arrangement of orientation pinwheel centers around area 17/18 transition zone in cat visual cortex. *Cereb. Cortex*, **10**, 593–601.

Ratzlaff, E.H. & Grinvald, A. (1991) A tandem-lens epifluorescence macroscope: hundred-fold brightness advantage for wide-field imaging. *J. Neurosci. Meth.*, **36**, 127–137.

Rosenquist, A.C., Edwards, S.B. & Palmer, L.A. (1974) An autoradiographic study of the projections of the dorsal lateral geniculate nucleus and the posterior nucleus in the cat. *Brain Res.*, **80**, 71–93.

Sanderson, K.J. (1971) The projection of the visual field to the lateral geniculate and medial interlaminar nuclei in the cat. *J. Comp. Neurol.*, **143**, 101–108.

Shmuel, A. & Grinvald, A. (1996) Functional organization for direction of motion and its relationship to orientation maps in cat area 18. *J. Neurosci.*, **16**, 6945–6964.

Shmuel, A. & Grinvald, A. (2000) Coexistence of linear zones and pinwheels within orientation maps in cat visual cortex. *Proc. Natl Acad. Sci. USA*, **97**, 5568–5573.

Swindale, N.V. (1991) Coverage and the design of striate cortex. *Biol. Cybern.*, **65**, 415–424.

Swindale, N.V., Matsubara, J.A. & Cynader, M.S. (1987) Surface organization of orientation and direction selectivity in cat area 18. *J. Neurosci.*, **7**, 1414–1427.

Swindale, N.V., Shoham, D., Grinvald, A., Bonhoeffer, T. & Hübener, M. (2000) Visual cortex maps are optimized for uniform coverage. *Nature Neurosci.*, **3**, 822–826.

Talbot, S.A. & Marshall, W.H. (1941) Physiological studies of neuronal mechanisms of visual localization and discrimination. *Am. J. Ophtalmol.*, **24**, 1255–1264.

Tusa, R.J., Palmer, L.A. & Rosenquist, A.C. (1978) The retinotopic organization of area 17 (striate cortex) in the cat. *J. Comp. Neurol.*, **177**, 213–236.

Tusa, R.J., Rosenquist, A.C. & Palmer, L.A. (1979) Retinotopic organisation of areas 18 and 19 in the cat. *J. Comp. Neurol.*, **185**, 657–678.

Vidyasagar, T.R., Pei, X. & Volgushev, M. (1996) Multiple mechanisms underlying the orientation selectivity of visual cortical neurones. *Trends in Neurosci.*, **19**, 272–277.

Warren, D.J., Fernandez, E. & Normann, R.A. (2001) High-resolution two-dimensional spatial mapping of cat striate cortex using a 100-microelectrode array. *Neuroscience*, **105**, 19–31.

Zar, J.H. (1999) *Biostatistical Analysis*. Prentice Hall, Upper Saddle River.